ARTICLE OPEN

Reprogramming the tumor microenvironment with antibody against membrane-proximal AXL to overcome immune checkpoint blockade resistance

Zuming Yang[1,2,3,4], Shuaishuai Cao[2,3,5], Jiaen Zhang[6], Xiaohua Nie[1], Zhimin Wang[1], Shaojun Yang[1,4], Jingshu Wang[1], Xin Sun[2,3], Xueli Kuang[2,3], Huiming Huang[2,3], Zifan Wei[1,4], Pengfei Duan[2,3], Mingwan Tang[2,3], Liyu Zhang[7], Zhenhua Ren[8], Xun Lan[2,3], Yang-Xin Fu[2,3,8]✉, Liguo Zhang[1,4]✉, Xuyuan Zhang[1]✉ and Yong Liang[2,3,8]✉

Immune-cold tumors fail to respond to immunotherapy due to insufficient lymphocyte infiltration within the tumor tissue. Increasing the objective response rate remains an urgent challenge. Here, we report the development of a monoclonal antibody (6C5) that specifically targets the membrane-proximal epitope of the receptor tyrosine kinase AXL and modulates antitumor immunity. Unlike traditional membrane-distal AXL antibodies, which suppress tumor growth primarily by blocking AXL signaling, 6C5 significantly enhanced innate immune sensing by promoting macrophage-mediated antigen uptake and type I interferon production. These effects further activated dendritic cells and increased $CD8^+$ T-cell infiltration and effector function, thereby reshaping the tumor microenvironment. However, AXL antibody treatment concurrently induced a suppressive subset of PD-$1^{hi}Foxp3^-CD4^+$ T cells. These cells displayed a transcriptomic profile resembling that of Tregs, characterized by elevated expression of immune checkpoint molecules (including PD-1 and CTLA4), reduced IL-2 production, and increased IL-2 receptor expression, thereby attenuating antitumor immune responses. The combination of 6C5 with dual immune checkpoint blockade (anti-PD-1 plus anti-CTLA-4) or a PD-1-targeted IL-2 fusion protein therapy mitigated this immunosuppression, resulting in potent tumor regression and durable immune memory. Our findings demonstrate that a membrane-proximal AXL-targeting antibody effectively converts the immune-cold tumor microenvironment, overcoming resistance to both conventional and next-generation immune checkpoint inhibitors.

Signal Transduction and Targeted Therapy (2026)11:139 ; https://doi.org/10.1038/s41392-026-02664-x

INTRODUCTION

Immune checkpoint inhibitors (ICIs) targeting programmed cell death protein 1 (PD-1) and cytotoxic T-lymphocyte-associated antigen 4 (CTLA-4) have revolutionized cancer treatment by blocking inhibitory pathways that negatively regulate T-cell activation and effector functions.[1] Despite these advances, durable clinical responses are achieved in only a minority of patients, predominantly those with immune-inflamed tumors.[2] A primary obstacle to broader ICI efficacy is the prevalence of immune-cold tumors, where the absence of tumor-specific cytotoxic T lymphocyte (CTL) induction and infiltration within the tumor microenvironment (TME) leads to primary resistance.[3] Numerous studies have shown that innate sensing plays a crucial role in inducing and reactivating tumor-specific T cells and facilitates tumor control.[4] Upon recognition of damage-associated molecular patterns or tumor-derived nucleic acids, innate sensors trigger the production of type I interferons (IFN-I) and proinflammatory cytokines. These cytokines are essential for the maturation and activation of antigen-presenting cells (APCs) by upregulating MHC class I/II, costimulatory molecules (CD80/CD86), and chemokine receptors, thereby enhancing cross-presentation of tumor antigens and priming of antigen-specific $CD8^+$ T cells for effective antitumor immunity.[5]

In the TME of immune-cold tumors, multiple immunosuppressive signals converge to dampen innate immune activation, severely limiting responsiveness to ICIs. Among these, AXL—a member of the TAM (TYRO3, AXL, MER) receptor tyrosine kinase family—has emerged as a pivotal negative regulator of innate immunity.[6] AXL is expressed on M2-like tumor-associated macrophages (TAMs) and dendritic cells (DCs). Engagement of AXL by its ligand GAS6 activates downstream signaling pathways in DCs, which induce the expression of suppressor of cytokine signaling proteins and attenuate pattern recognition receptor-mediated signaling. This signaling axis inhibits interferon regulatory factor- or NF-κB-dependent transcription, thereby suppressing type I interferons and proinflammatory cytokine expression, ultimately

[1]State Key Laboratory of Biomacromolecules, Institute of Biophysics, Chinese Academy of Sciences, Beijing, China; [2]Center for Cancer Biology, School of Basic Medical Sciences, Tsinghua University, Beijing, China; [3]State Key Laboratory of Molecular oncology, Tsinghua University, Beijing, China; [4]University of Chinese Academy of Sciences, Beijing, China; [5]State Key Laboratory of Biopharmaceutical Preparation and Delivery, Institute of Process Engineering, Chinese Academy of Sciences, Beijing, China; [6]Department of Urology, Peking University First Hospital, Beijing, China; [7]Senior Department of General Surgery, Chinese PLA General Hospital, Beijing, China and [8]Changping Laboratory, Beijing, China Correspondence: Yang-Xin Fu (yangxinfu@tsinghua.edu.cn) or Liguo Zhang (liguozhang@ibp.ac.cn) or Xuyuan Zhang (zxy_better@ibp.ac.cn) or Yong Liang (yongliang@tsinghua.edu.cn)
These authors contributed equally: Zuming Yang, Shuaishuai Cao

Received: 13 June 2025 Revised: 25 December 2025 Accepted: 2 March 2026
Published online: 17 April 2026

driving DCs toward a tolerogenic phenotype.[7] AXL-expressing M2-like macrophages exhibit upregulated PD-L1 expression, which induces secretion of immunosuppressive cytokines,[8] thus acting as a negative regulator of innate sensing. A positive correlation exists between AXL and PD-L1 expression, which has been linked to both intrinsic and acquired resistance to radiation or PD-1 blockade.[9,10] Beyond its immunomodulatory role in myeloid cells, AXL is also highly expressed in a wide range of malignancies, including non-small cell lung cancer,[11] renal cell carcinoma,[12] gastric cancer,[13] ovarian cancer,[14] breast cancer,[15] and melanoma,[16] where its overexpression correlates with poor prognosis, metastasis, and resistance to ICIs.[6] Structurally, AXL comprises two immunoglobulin-like (Ig-like) domains and two fibronectin type III (FNIII) domains. Its ligand, GAS6, binds to the first Ig-like domain in the membrane-distal region of AXL, inducing dimerization and activating downstream signaling pathways such as phosphatidylinositol 3-kinase/Akt kinase and mitogen-activated protein kinase/extracellular signal-regulated kinase that promote tumor cell growth and metastasis.[8,17] Consequently, AXL inhibition offers a dual therapeutic advantage by alleviating myeloid-mediated immunosuppression and directly inhibiting tumor progression, positioning AXL as a compelling target to enhance ICIs' efficacy in resistant cancers.

Various small-molecule inhibitors and biologics that target AXL have been developed to block AXL in cancer therapy.[18–22] Most biologics, such as antibodies and decoy receptors, are designed to bind membrane-distal epitopes and compete with the GAS6–AXL interaction.[21,23,24] However, these strategies have shown limited clinical efficacy, likely because of incomplete AXL blockade or a lack of effective engagement with immune activation pathways. For example, the decoy receptor AVB-S6-500 failed to meet its endpoint in a phase III clinical trial for ovarian cancer (NCT04729608). Moreover, the widespread expression of AXL in normal tissues and immune cells raises substantial concerns of off-target toxicity for AXL-directed antibody–drug conjugate (ADC). Enapotamab Vedotin, which advanced into clinical development, was discontinued due to its significant adverse effects observed in clinical trials.[6] Moreover, beyond signaling blockade, antibodies can exert potent antitumor effects through Fc-mediated mechanisms such as antibody-dependent cellular cytotoxicity (ADCC) and antibody-dependent cellular phagocytosis (ADCP). These processes enhance tumor antigen uptake by APCs, stimulate type I IFN production, and facilitate T-cell priming, thereby bridging innate immune activation with the induction of adaptive antitumor immunity.[25] However, the potential contribution of antibodies to mediate tumor control during the development of AXL antibodies via the ADCP/ADCC remains unclear.

In this study, we report that 6C5, a monoclonal antibody that targets the membrane-proximal epitope of AXL, enhanced the macrophage-mediated ADCP effect and facilitated the uptake and presentation of tumor antigens. This process further activated the type I interferon pathway and promoted T-cell-dependent antitumor immunity, effectively overcoming resistance to ICIs (anti-PD-1 plus anti-CTLA-4) in immune-cold melanoma models. Moreover, the combinatorial regimen incorporating a PD-1-targeted IL-2 fusion protein exhibited a robust capacity to evoke a durable immune memory response, which is crucial for the sustained suppression of tumor recurrence.

RESULTS

An antibody targeting the membrane-proximal epitope of AXL has enhanced antitumor efficacy

To explore the therapeutic potential of antibodies targeting distinct AXL epitopes, we developed several monoclonal antibodies against human AXL (hAXL). Clones 9# and 13# were found to bind the first Ig-like domain (domain 1), corresponding to membrane-distal epitopes. Clone 9# competes with the ligand GAS6 for binding to AXL, whereas clone 13# does not.[26] In contrast, clone 6C5 binds to the second FNIII domain (domain 4), which represents a membrane-proximal epitope (Fig. 1a, Supplementary Fig. 1a, b). Compared with clones 9# and 13#, 6C5 exhibited stronger binding to hAXL on the cell membrane surface (Fig. 1b). Furthermore, we demonstrated that 6C5 binds to native AXL on primary human myeloid cells (Supplementary Fig. 1c). To evaluate the in vivo therapeutic efficacy of these antibodies, we engineered a B16-hAXL melanoma cell line by stably expressing hAXL in B16F10 mouse melanoma cells (Supplementary Fig. 1d). In a syngeneic mouse model, treatment with 6C5 exhibited significant therapeutic efficacy against subcutaneous B16-hAXL melanoma in both female and male mice (Fig. 1c and Supplementary Fig. 1e, f). Immunohistochemical analysis revealed no apparent histopathological abnormalities in major organs following 6C5 treatment (Supplementary Fig. 1g), and serum cytokine levels remained comparable to those in control mice (Supplementary Fig. 1h), indicating that 6C5 treatment did not induce systemic toxicity. Furthermore, 6C5 also potently inhibited the growth of CT26-hAXL colon tumors in BALB/c mice (Supplementary Fig. 1i), supporting its broad antitumor activity across different tumor types. We also tested the YW327.6S2 (6S2) antibody, developed by Genentech, which targets the first Ig-like domain and competes with GAS6 for AXL binding[23] (Fig. 1a). 6S2 and 6C5 exhibited comparable binding affinities for hAXL (Fig. 1d). Notably, in vivo, compared with 6S2, 6C5 showed significantly superior antitumor efficacy in the syngeneic melanoma model (Fig. 1e, f). These results suggest that targeting the membrane-proximal epitope of AXL with 6C5 confers enhanced therapeutic benefit over the use of antibodies directed against membrane-distal domains.

The therapeutic efficacy of 6C5 is dependent on its binding to AXL on tumor cells

Inoculation of murine tumor cells expressing hAXL into wild-type mice may trigger xenogeneic immunogenic responses, potentially confounding the evaluation of antibody-based therapies. To enable a more accurate assessment, we generated hAXL-transgenic C57BL/6 mice ($hAXL^{BAC}$ mice) expressing hAXL (Supplementary Fig. 2a). Flow cytometric analysis of splenocytes confirmed hAXL expression predominantly in $CD11c^+$ cells (Fig. 2a and Supplementary Fig. 2b), mimicking the expression pattern of AXL in human immune compartments and thereby increasing the translational relevance of the model. Using these transgenic mice, we compared the therapeutic efficacy of the 6C5 and 6S2 antibodies. 6C5 consistently outperformed 6S2 in suppressing B16-hAXL tumor growth (Fig. 2b). To further evaluate the cross-tumor applicability of 6C5 in $hAXL^{BAC}$ mice, we engineered an MC38-hAXL colon tumor cell line (Supplementary Fig. 2c). In $hAXL^{BAC}$ mice, compared with 6S2, 6C5 also demonstrated enhanced efficacy in inhibiting the growth of MC38-hAXL tumors (Fig. 2c). Given that most cancer-related deaths result from metastasis, we next explored the ability of 6C5 to control metastatic disease. In a lung metastasis model established by intravenous injection of B16-hAXL cells, 6C5-treated mice exhibited a marked reduction in metastatic nodules compared to the control group (Fig. 2d), indicating robust inhibition of metastatic tumor growth. Finally, to explore its translational potential in human cancers, we tested a chimeric 6C5 antibody version in humanized mouse models. The chimeric 6C5 effectively suppressed the growth of human pancreatic ductal adenocarcinoma CFPAC-1 tumors (Fig. 2e).

Because AXL is also present on host cells, such as M2 macrophages[6,27] and DCs,[28] we investigated whether the efficacy of 6C5 involves targeting the host's AXL. 6C5 was found to bind murine AXL (mAXL) but with weak affinity (Supplementary Fig. 2d). The antibody retained antitumor efficacy in Axl-knockout mice, indicating that host AXL expression is not necessary (Fig. 2f).

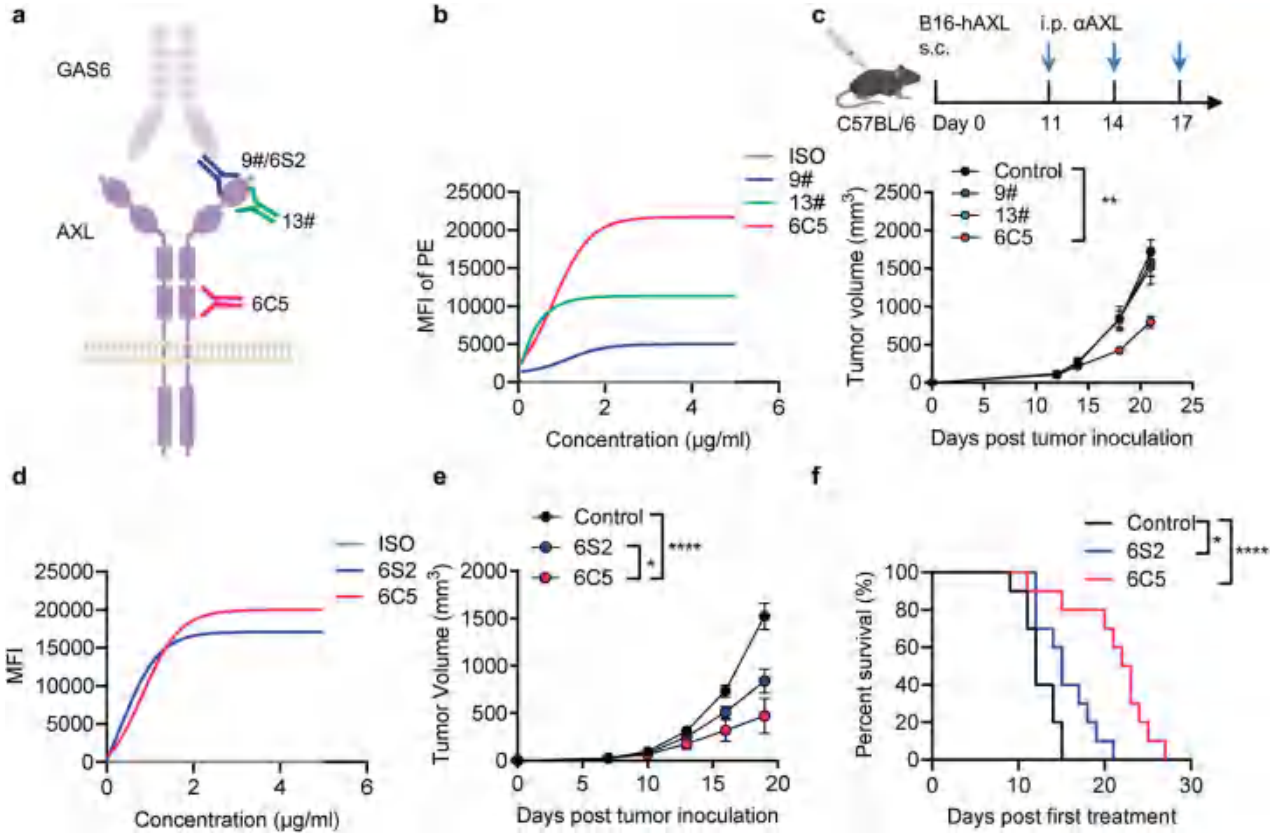

Fig. 1 An antibody targeting the membrane-proximal epitope of AXL has enhanced antitumor efficacy. a Schematic depiction of antibodies that bind to different epitopes of AXL. b Comparison of the binding affinities of anti-AXL antibodies for AXL on the cell surface. c Tumor growth curves of B16-hAXL-bearing female C57BL/6 mice (n = 5) treated with PBS (control), 9#, 13#, or 6C5 by intraperitoneal injection on days 11, 14, and 17. d Comparison of the binding affinities of 6S2 and 6C5 to AXL on the cell surface. Tumor growth curves (e) and survival curves (f) of B16-hAXL-bearing C57BL/6 mice (n = 10) treated with PBS (control), 6S2 or 6C5 cells by intraperitoneal injection on days 8, 11, 14, and 17. The data are presented as the means ± SEMs of two or three independent experiments. Statistical analysis of tumor growth was performed via two-way ANOVA. For the survival curve data in (f), the log-rank test was applied. ns (not significant), *P < 0.05, **P < 0.01 and ****P < 0.0001

In contrast, 6C5 had no therapeutic benefit in tumors lacking hAXL, highlighting the necessity of AXL expression on tumor cells (Fig. 2g). The activation of AXL signaling has been demonstrated to promote tumor progression.[29] We next examined whether 6C5 exerts a direct effect on tumor cell proliferation. In vitro treatment of B16-hAXL melanoma cells with 6C5 showed no growth inhibition (Supplementary Fig. 2e). Similar results were observed in the AXL-high human tumor cell lines SN12C and Calu-1; only cabozantinib, a tyrosine kinase inhibitor, significantly inhibited proliferation, whereas 6C5 did not (Supplementary Fig. 2f, g). Moreover, in vitro treatment with these AXL antibodies increased the phosphorylation of AXL and its downstream Akt effector molecules in cancer cells, suggesting that they do not block but rather activate AXL signaling (Supplementary Fig. 2h). Interestingly, both the 6C5 antibody and its counterpart antibody 1# led to a decrease in the classical AXL band at approximately 140 kDa along with a concurrent increase in the lower 100 kDa molecular band, suggesting a possible modification change or truncation of AXL molecules after treatment with these antibodies (Supplementary Fig. 2h). These findings suggest that the efficacy of the 6C5 antibody depends on its interaction with AXL on tumor cells, but it does not directly affect tumor growth through the modulation of AXL signaling.

Given the lack of direct cytotoxicity, we hypothesized that 6C5 mediates tumor control via immune mechanisms. In support of this finding, 6C5 failed to control B16-hAXL tumor growth in immunodeficient Rag1$^{-/-}$ and NSG-SGM3 mice, which lack functional T and B cells (Fig. 2h and Supplementary Fig. 2i). These data demonstrate that the therapeutic efficacy of 6C5 requires adaptive immunity and is dependent on AXL expression on tumor cells.

AXL Ab treatment modulates the TME to increase TIICs infiltration and antitumor CD8$^+$ T immunity

Given that adaptive immunity is required for AXL Ab-mediated tumor control, we further investigated changes in tumor-infiltrating immune cells (TIICs). We sorted intratumoral CD45$^+$ cells from treated tumors and conducted single-cell sequencing to analyze their phenotypic and transcriptional landscape. Unsupervised clustering identified 22 distinct immune cell clusters, which were visualized via UMAP (Supplementary Fig. 3a). Macrophages and monocytes (clusters 0, 1, 2, 4, 5, 6, 7, 8, and 10) constitute the majority of TIICs (Supplementary Fig. 3a, b). Moreover, substantial upregulation of distinct chemokine profiles was observed in TAMs following 6C5 treatment (Fig. 3a). These findings suggest that 6C5 promotes a proinflammatory myeloid phenotype, which may enhance immune cell infiltration. To confirm this, we next performed flow cytometric analysis of TIICs. Indeed, following 6C5 treatment, multiple myeloid and lymphoid populations, including DCs, monocytes, neutrophils, T cells, and B cells, were increased within the tumor (Fig. 3b, c), indicating effective remodeling of the TME toward a more immunologically "hot" phenotype. Consistently, immunofluorescence analysis of intratumoral CD45$^+$ leukocytes and CD8$^+$ T cells further confirmed that 6C5 treatment markedly enhanced immune cell infiltration within the tumor (Supplementary Fig. 3c).

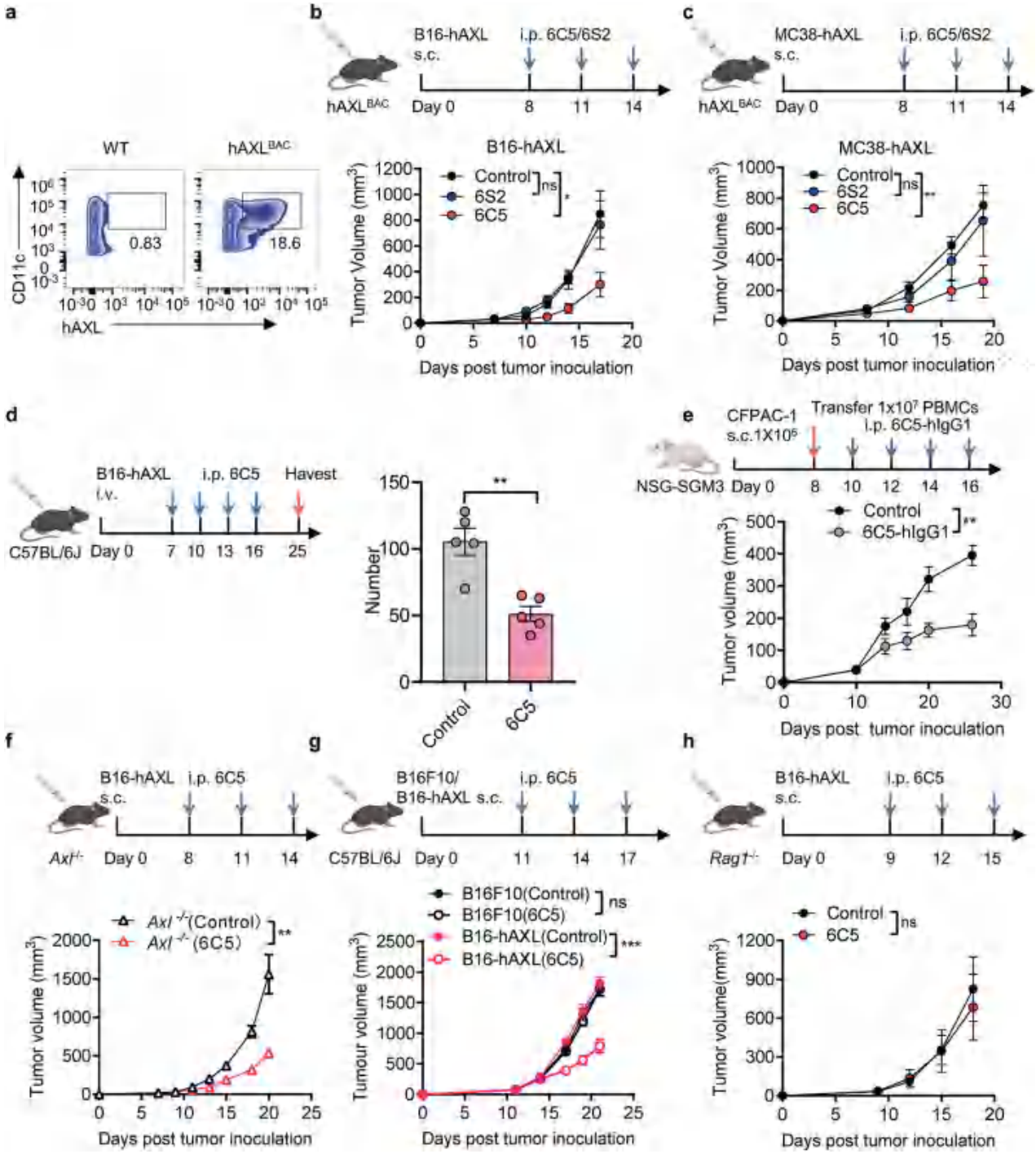

Fig. 2 The therapeutic effect of 6C5 is dependent on its binding to AXL on tumor cells. a Flow cytometry was conducted to evaluate the expression of hAXL in splenocytes isolated from hAXL-transgenic mice ($hAXL^{BAC}$ mice). b Tumor growth curves of B16-hAXL-bearing hAXL-transgenic mice (n = 5) treated with PBS (control), 6C5, or 6S2 by intraperitoneal injection on days 8, 11, and 14. c Tumor growth curves of MC38-hAXL-bearing hAXL-transgenic mice (n = 5) treated with PBS (control), 6C5, or 6S2 by intraperitoneal injection on days 8, 11, and 14. d C57BL/6J mice (n = 5) were intravenously inoculated with 2×10^6 B16-hAXL cells. Tumor-bearing mice received intraperitoneal injections of 6C5 (200 μg per mouse) on days 7, 10, 13, and 16 post-inoculation. Lungs were collected on day 18 following the first administration for tumor metastasis analysis. e NSG-SGM3 mice (n = 6) were inoculated with 1×10^6 CFPAC-1 cells. On day 8 post-inoculation, the tumor-bearing mice received an intravenous injection of 1×10^7 human PBMCs, followed by the intraperitoneal administration of PBS (control) or 6C5-hIgG1 (200 μg per mouse) on day 10 and treatment every two days. f Tumor growth curves of B16-hAXL-bearing $Axl^{-/-}$ C57BL/6 mice (n = 6) treated with PBS (control) or 6C5 by intraperitoneal injection on days 8, 11, and 14. g Tumor growth curves of B16F10- or B16-hAXL-bearing C57BL/6 mice (n = 6) treated with PBS (control) or 6C5 by intraperitoneal injection on days 11, 14, and 17. h Tumor growth curves of B16-hAXL-bearing $Rag1^{-/-}$ mice treated with PBS (control, n = 4) or 6C5 (n = 5) by intraperitoneal injection on days 9, 12, and 15. The data are presented as the means ± SEMs, and two or three independent experiments were performed. Statistical analysis of tumor growth was performed via two-way ANOVA. For (d), unpaired two-tailed t-tests were applied. ns (not significant), *P < 0.05, **P < 0.01, ***P < 0.001

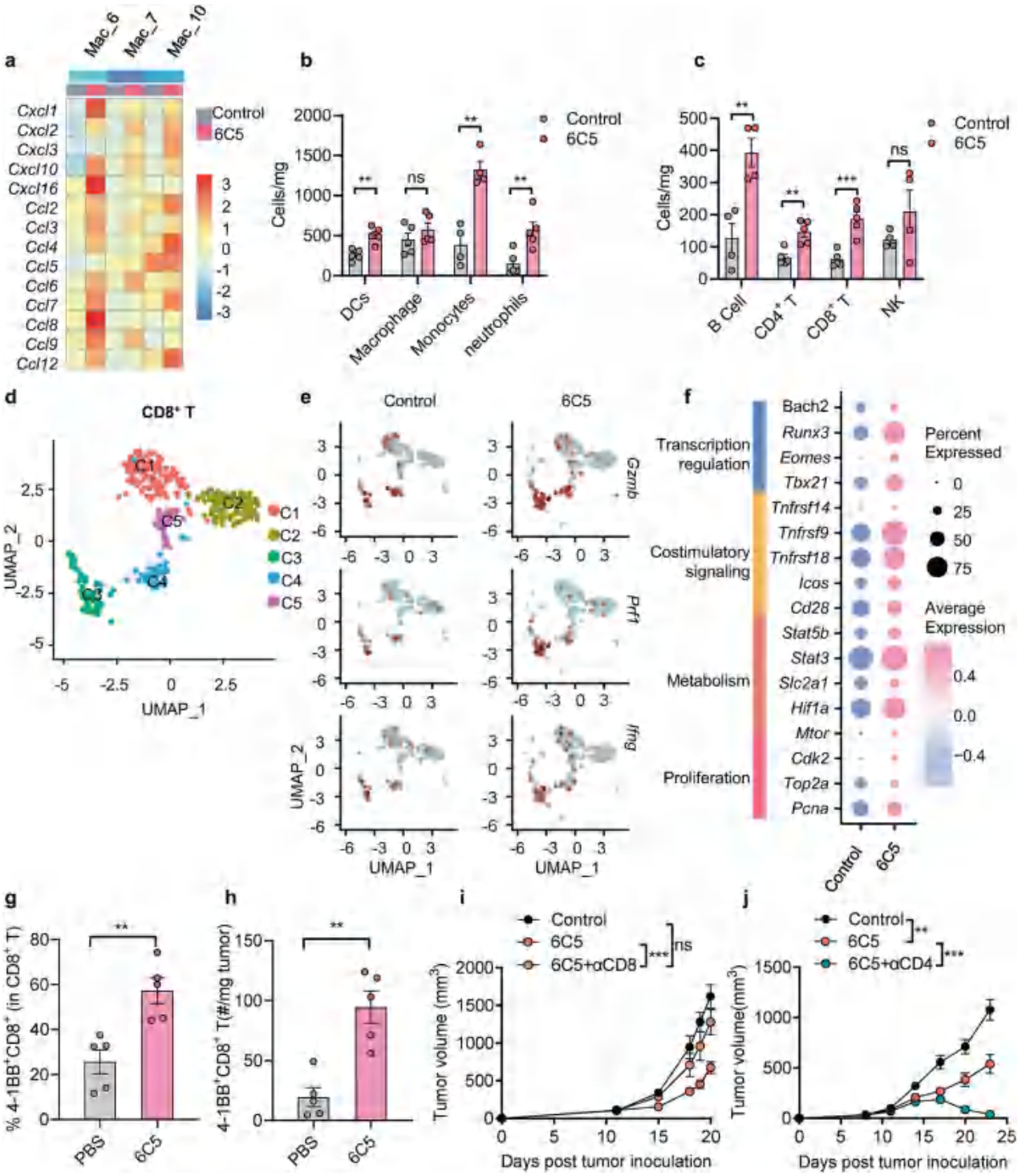

Fig. 3 AXL Ab treatment modulates the TME to increase TIIC infiltration and antitumor CD8$^+$ T immunity. a Heatmap showing unsupervised hierarchical clustering of chemokine gene expression profiles in macrophage populations. The number of intratumoral myeloid (b) and lymphoid immune (c) cells was analyzed on day 17 in B16-hAXL-bearing C57BL/6 mice that were treated intraperitoneally with 6C5 on days 12 and 15. d Uniform manifold approximation and projection (UMAP) analysis of total CD8$^+$ T cells in tumors. e FeaturePlot visualization of effector molecule expression in intratumoral CD8$^+$ T cells from the control and 6C5-treated groups. f Dot plot of genes associated with T-cell proliferation, metabolism, costimulatory signaling, and transcriptional regulation in Cluster 3 CD8$^+$ T cells from the control and 6C5-treated groups. The frequency (g) and quantity (h) of intratumoral 4-1BB$^+$CD8$^+$ T cells were analyzed on day 15 in B16-hAXL-bearing C57BL/6 mice that were treated intraperitoneally with 6C5 on days 11 and 14. i Tumor growth curves of B16-hAXL-bearing C57BL/6 mice (n = 5) treated with PBS (control), 6C5 or 6C5 combined with an anti-CD8 antibody (αCD8). j Tumor growth curves of B16-hAXL-bearing C57BL/6 mice (n = 10) treated with PBS (control), 6C5 or 6C5 combined with an anti-CD4 antibody (αCD4). The data are presented as the means ± SEMs, and two or three independent experiments were performed. Statistical analysis of tumor growth was performed via two-way ANOVA. For (b, c, g, h), unpaired two-tailed t-tests were applied. ns not significant, *$P < 0.05$, **$P < 0.01$, and ***$P < 0.001$

Given the critical role of $CD8^+$ T cells in antitumor immunity, we further classified $CD3^+CD8^+$ T cells from total immune cells. Five distinct subpopulations (C1–C5) were identified and visualized via UMAP for dimensionality reduction (Fig. 3d and Supplementary Fig. 3d). Among the $CD8^+$ T-cell subsets, Cluster 3 (C3) was distinguished by high expression of effector genes (Gzmb, Prf1 and Ifng), indicating a cytotoxic function (Fig. 3e). Notably, 6C5 treatment increased both the abundance and effector activity of this cluster within the $CD8^+$ T-cell compartment (Fig. 3e and Supplementary Fig. 3e). Additionally, 6C5 treatment upregulated genes associated with T-cell proliferation (Top2a, Pcna, and Cdk2), metabolism (Mtor, Hif1a, Slc2a1, Stat3, and Stat5b), costimulatory signaling (Cd28, Icos, Tnfrsf9, Tnfrsf14, and Tnfrsf18), and transcription regulation (Tbx21, Eomes, Runx3, and Bach2) in C3 (Fig. 3f). This population expressed high levels of 4-1BB (Tnfrsf9) and was thus designated $4\text{-}1BB^+CD8^+$ T cells (Supplementary Fig. 3f). We further analyzed the impact of 6C5 treatment on intratumoral $4\text{-}1BB^+CD8^+$ T cells via flow cytometry (Supplementary Fig. 3g). Flow cytometric analysis confirmed a substantial increase in both the frequency and number of these effector $CD8^+$ T cells after 6C5 treatment (Fig. 3g, h). To directly assess their role, we depleted $CD8^+$ T cells during therapy. $CD8^+$ T-cell depletion completely abolished the antitumor activity of 6C5, confirming its essential role in mediating therapeutic efficacy (Fig. 3i and Supplementary Fig. 3h). While $CD8^+$ T cells are typically supported by $CD4^+$ T cells,[30,31] we surprisingly found that depleting $CD4^+$ T cells enhanced 6C5 efficacy (Fig. 3j and Supplementary Fig. 3i), suggesting the induction of an immunosuppressive $CD4^+$ T-cell subset following 6C5 treatment.

Membrane-proximal-targeting AXL Ab activates APCs for tumor control with potent ADCP induction ability

Considering the critical role of $CD8^+$ T cells in mediating effective anti-AXL therapy, we next investigated the mechanisms by which anti-AXL enhances T-cell responses. Engagement of activated Fc receptors (FcγRs) on APCs via the antibody Fc domain could induce phagocytosis of target tumor cells and subsequent cross-presentation of tumor antigens to activate $CD8^+$ T cells. In addition, Fc-mediated effector functions may trigger ADCC through natural killer (NK) cells to kill tumor cells. To delineate the immune effector mechanisms involved, we performed selective immune cell depletion experiments. While depletion of NK cells did not affect tumor control, the therapeutic efficacy of the 6C5 antibody was completely abolished after macrophage depletion, indicating that macrophages, but not NK cells, are essential mediators of 6C5-induced tumor control (Fig. 4a–c and Supplementary Fig. 4a, b). Next, we investigated the impact of the 6C5 antibody on the phagocytosis of tumor cell antigens by macrophages. Tumor cells were labeled with CFSE and subsequently incubated with macrophages. Flow cytometry analysis revealed that the addition of the 6C5 antibody significantly enhanced the phagocytic ability of the macrophages (Fig. 4d and Supplementary Fig. 4c). In contrast, the Fc variant of 6C5 that lacks the ability to bind FcγR exhibited minimal phagocytic activity (Fig. 4d and Supplementary Fig. 4c) and completely lost its antitumor efficacy (Fig. 4e). These results illustrate the critical role of Fc-dependent macrophage engagement in AXL Ab-mediated tumor control.

We hypothesized that variations in the abilities of different anti-AXL monoclonal antibodies to induce ADCP activity may be attributed to their different epitope targeting abilities, ultimately leading to distinct therapeutic efficacy. To test this hypothesis, we compared several anti-AXL antibodies that target either membrane-proximal (the second FNIII domain) or membrane-distal epitopes (the first Ig-like domain) (Supplementary Fig. 1a, b). Antibodies (1#, 20#, and 22#) targeting the membrane-proximal epitopes of AXL potently induced macrophage-mediated phagocytosis of tumor antigens, demonstrating an efficiency comparable to that of 6C5 and surpassing the effectiveness of antibodies (9#, 13#, and 6S2) targeting membrane-distal epitopes (Fig. 4f and Supplementary Fig. 4d). Moreover, in vivo treatment with antibodies (1#, 20#) targeting the membrane-proximal epitopes significantly inhibited the growth of B16-hAXL melanoma (Supplementary Fig. 4e), indicating that the increased ADCP induced by the binding of antibodies to the membrane-proximal epitopes of AXL is associated with improved therapeutic outcomes.

Finally, whether macrophages can directly function as APCs to activate $CD8^+$ T cells or require the involvement of DCs remains unclear. To address this question, we treated $Batf3^{-/-}$ mice, which specifically lack type 1 conventional dendritic cells (cDC1s), with a 6C5 antibody and observed a decrease in antitumor efficacy (Supplementary Fig. 4f). Similarly, depletion of DC cells by diphtheria toxin (DT) impaired AXL antibody-mediated tumor control in CD11c-DTR mice (Fig. 4g). Collectively, these findings indicate that the therapeutic efficacy of 6C5 is dependent on APCs, including both macrophages and DCs.

AXL Ab treatment activates type I interferon signaling in APCs to trigger antitumor immunity

Type I interferons are essential for the cross-priming of $CD8^+$ T cells by APCs.[32] Single-cell RNA-sequencing of tumors treated with 6C5 revealed broad upregulation of interferon-stimulated genes (ISGs) in both the macrophage and DC subsets (Fig. 5a). Further analysis revealed that IFN-β was the dominant subtype expressed, primarily by monocytes and macrophages (Fig. 5b and Supplementary Fig. 5a), whereas macrophages (clusters 0, 1, 2, 4, 6, 7, and 10), characterized by the expression of Adgre1, Cd68, and Fcgr1, constituted the majority of intratumoral immune cells (Fig. 5b and Supplementary Fig. 3b). These results identify macrophages as the principal intratumoral source of IFN-I. To investigate the effect of antibodies on IFN-β production by macrophages, we co-incubated macrophages with tumor cells in vitro with or without antibodies. After a 24-h incubation, the 6C5 antibody significantly upregulated IFN-β production in the incubation system (Fig. 5c). In contrast, the addition of an Fc-silencing 6C5 antibody did not increase IFN-β production compared with that in the control group (Fig. 5c). These findings collectively show that 6C5 promotes macrophage-mediated phagocytosis and IFN-I secretion.

To determine whether IFN-I induction is essential for tumor control, we used $Ifnar1^{-/-}$ mice. Indeed, 6C5 Ab treatment failed to inhibit tumor growth in $Ifnar1^{-/-}$ mice (Supplementary Fig. 5b). Similarly, blocking the IFN-I pathway in WT mice with an antibody impaired 6C5 antibody-mediated tumor control (Fig. 5d), suggesting that the IFN-I pathway is critical for mediating tumor control. IFN-I can be derived from the activation of the STING (Tmem173) or MyD88 (Myd88) pathways.[33,34] In $Tmem173^{-/-}$ mice, the therapeutic efficacy of the 6C5 antibody was maintained (Fig. 5e). Conversely, the therapeutic effect of the antibody was entirely abolished in $Myd88^{-/-}$ mice (Fig. 5f). These results indicate that the 6C5 antibody induces IFN-I secretion via the MyD88 pathway for tumor control.

The activation of IFNAR signaling by IFN-I could promote the activation and antigen presentation of APCs, which further activate the T-cell response. Our single-cell RNA-sequencing data revealed that treatment with 6C5 led to the upregulation of several antigen presentation-related costimulatory molecules (Cd40, Cd80, Cd86, and Cd83), MHC molecules (H2-Eb1, H2-Eb2, H2-K1, and H2-D1), and migration markers (Icam1 and Ccr7) across several macrophage and DC subsets (Fig. 5g). These transcriptional changes suggest that 6C5 promote APC cell activation, increase their antigen-presenting capacity and their migratory potential. Next, we investigated which cell subset expressing IFNAR is required for tumor control during 6C5 antibody treatment. We crossed the $Ifnar1^{f/f}$ allele[35] onto the Zbtb46-cre

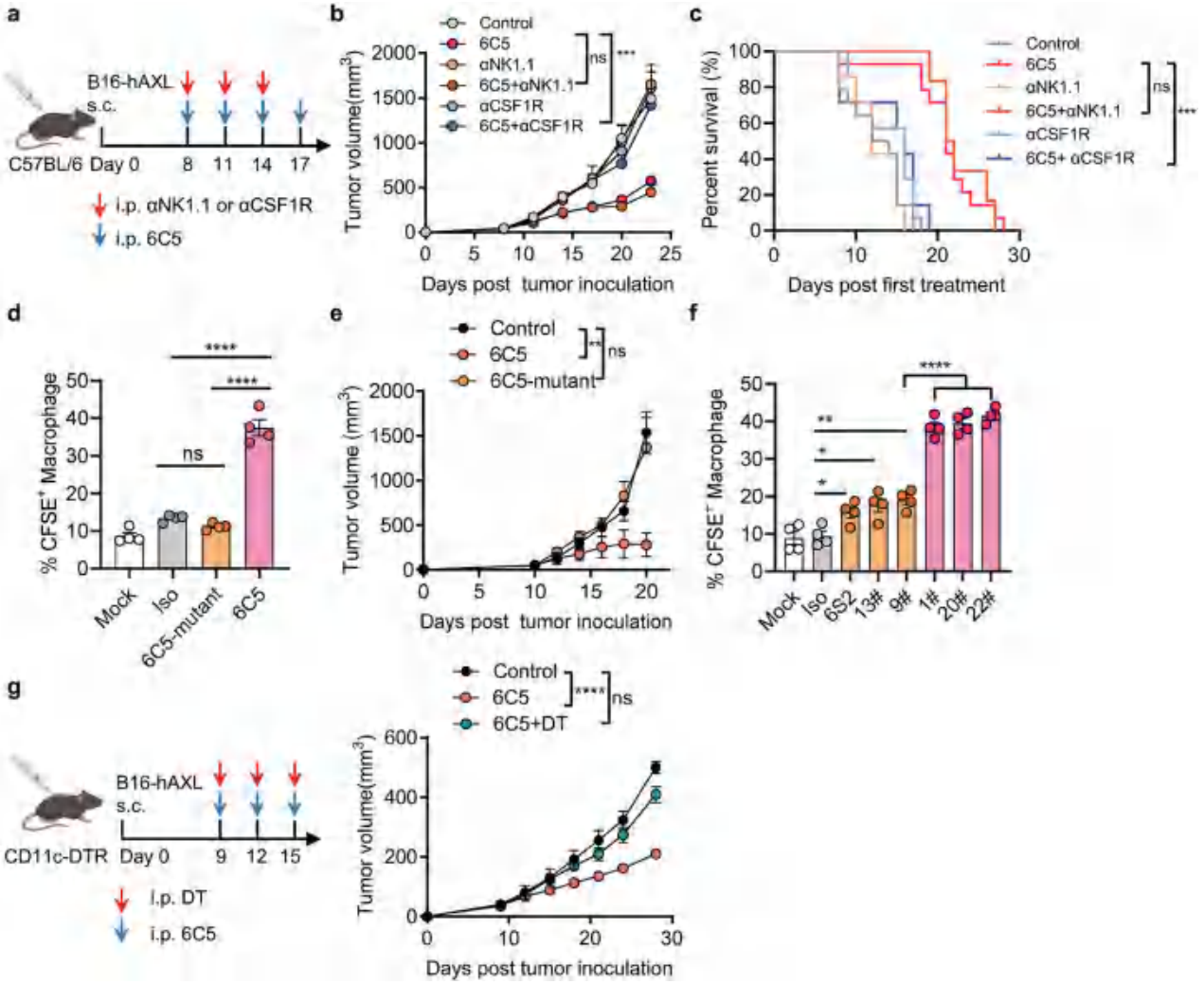

Fig. 4 Membrane-proximal targeting of the AXL Ab activates APCs for tumor control with potent ADCP induction ability. a Workflow for B16-hAXL tumor modeling with 6C5 + αNK1.1 or αCSF1R treatment. Tumor growth curves (b) and survival curves (c) of B16-hAXL-bearing C57BL/6 mice treated with PBS (control, n = 14), 6C5 (n = 14), αNK1.1 (n = 7), αCSF1R (n = 7), 6C5 + αNK1.1 (n = 6), or 6C5 + αCSF1R (n = 7). d The frequency of $CFSE^+$ macrophages was analyzed 2 h after coculture with B16-hAXL tumor cells and macrophages in vitro, both in the presence and absence of 6C5, Fc mutated variant 6C5 (6C5-mutant), or an isotype control (Iso). e Tumor growth curves of B16-hAXL-bearing C57BL/6 mice treated with PBS (control, n = 6), 6C5 (n = 6) or the 6C5-mutant (n = 5). f The frequency of $CFSE^+$ macrophages was analyzed 2 h after coculture with B16-hAXL tumor cells and macrophages in vitro, both in the presence and absence of the indicated antibodies. g Tumor growth curves of B16-hAXL-bearing CD11c-DTR C57BL/6 mice treated with control (PBS, n = 6), 6C5 (n = 7), or 6C5 + DT (n = 7) are shown. The data are presented as the means ± SEMs, and two or three independent experiments were performed. Statistical analysis of tumor growth was performed via two-way ANOVA. For the survival curve data in (c), the log-rank test was applied. ns (not significant), *P < 0.05, **P < 0.01 and ****P < 0.0001

and Lyz2-cre deletion strains[36,37]. The Zbtb46-cre $Ifnar1^{f/f}$ strain specifically deleted Ifnar1 within cDCs, whereas the Lyz2-cre $Ifnar1^{f/f}$ strain selectively deleted Ifnar1 in macrophages. Notably, 6C5-mediated tumor control was significantly impaired in Zbtb46-cre $Ifnar1^{f/f}$ mice (Fig. 5h), whereas 6C5 treatment was effective in Lyz2-cre $Ifnar1^{f/f}$ mice (Supplementary Fig. 5c). These findings demonstrate that the response of cDCs to IFN-I is essential for 6C5 treatment-induced antitumor immunity.

The 6C5 antibody overcomes melanoma resistance to immune checkpoint inhibitors

While 6C5 monotherapy resulted in significant tumor suppression, it failed to achieve complete tumor eradication. Investigations into resistance mechanisms revealed substantial loss of AXL expression in tumor cells during progression, with a more pronounced trend observed in animals treated with 6C5 (Supplementary Fig. 5d). These findings highlight the need for combination therapies to achieve durable therapeutic responses.

$CD4^+$ T cells expanded during 6C5 treatment and appeared to exert immunosuppressive effects (Fig. 3c, j). Tregs are typically considered the major suppressive $CD4^+$ T subset. However, combining the 6C5 Ab with an anti-CTLA-4 antibody failed to enhance therapeutic efficacy (Fig. 6a), suggesting that Tregs are not the primary mediators of immune suppression. The differences in gene expression patterns between $Foxp3^-CD4^+$ T cells from the 6C5-treated groups and those from the PBS-treated groups were positively correlated with the differences in gene expression between intratumoral Treg cells and $Foxp3^-CD4^+$ T cells from the PBS-treated group (Fig. 6b). These results suggested that intratumoral $Foxp3^-CD4^+$ T cells may adopt a transcriptional profile resembling that of Treg cells following 6C5 treatment. $PD\text{-}1^{hi}Foxp3^-CD4^+$ T cells were previously shown to be induced in association with immunosuppression by anti-CTLA-4 antibody treatment in melanoma.[38] Similarly, 6C5 treatment was associated with significant upregulation of $PD\text{-}1^{hi}Foxp3^-CD4^+$ T cells within the tumor (Fig. 6c). We observed that global differences in gene expression between PD-

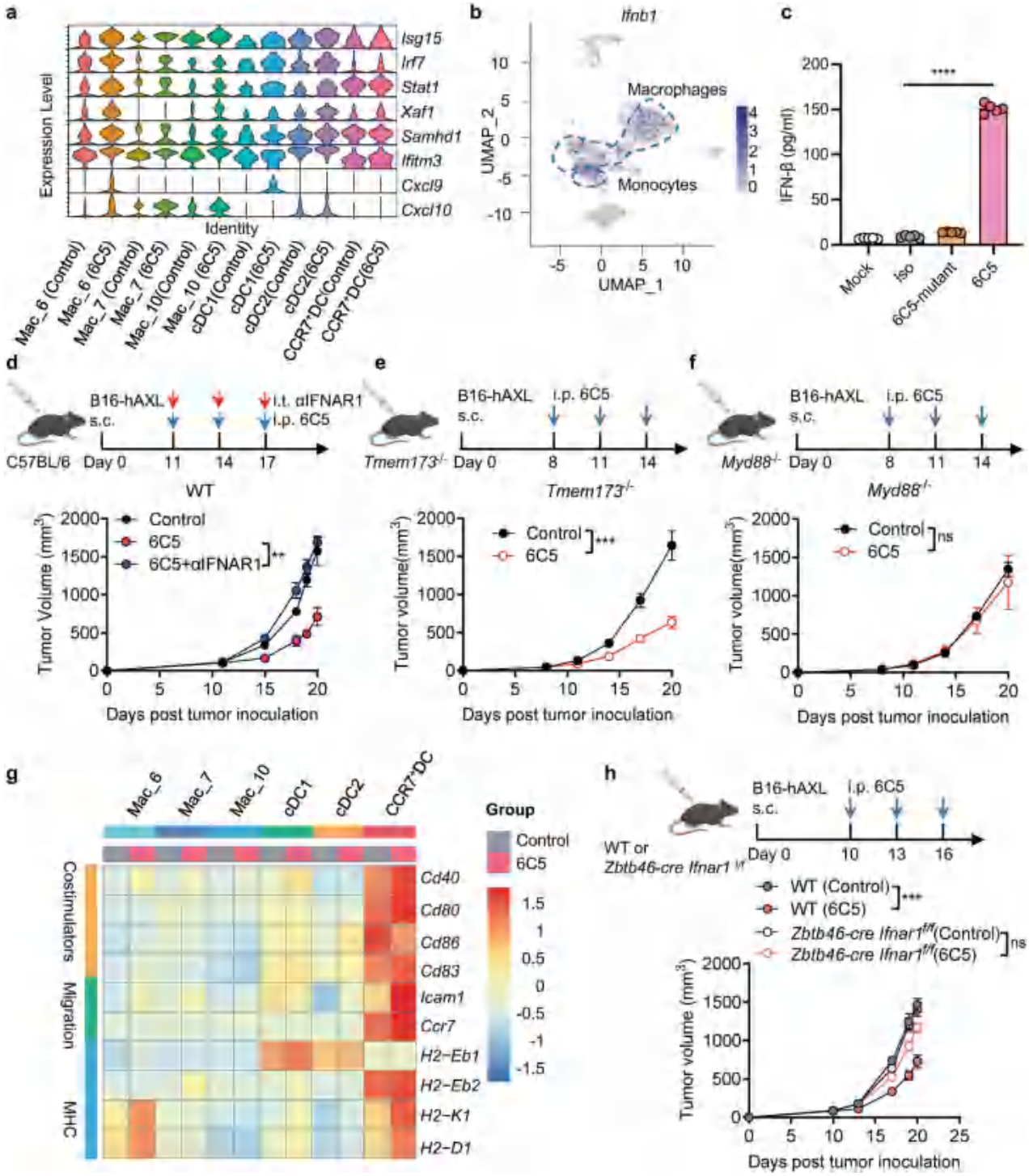

Fig. 5 AXL Ab treatment activates type I interferon signaling in APCs to trigger antitumor immunity. a Violin plots showing the expression levels of interferon-stimulated genes (ISGs) across different DC and macrophage subsets. b Feature plot showing the expression of Ifnb1 in immune cells. c IFN-β in the supernatant was analyzed in macrophages and the B16-hAXL tumor cell coculture system in the presence and absence of the indicated antibodies. d Tumor growth curves of B16-hAXL-bearing C57BL/6 mice (n = 5) treated with PBS (control), 6C5, or 6C5 + αIFNAR1. e Tumor growth curves of B16-hAXL-bearing Tmem173$^{-/-}$ mice treated with PBS (control, n = 5) or 6C5 (n = 6). f Tumor growth curves of B16-hAXL-bearing Myd88$^{-/-}$ mice treated with PBS (control, n = 5) or 6C5 cells (n = 6). g Heatmap showing changes in the expression of antigen presentation- and migration-related genes in macrophage and dendritic cell (DC) subsets between the 6C5-treated and control groups. h Tumor growth curves of B16-hAXL-bearing C57BL/6 mice (n = 5) and Zbtb46-cre Ifnar1$^{f/f}$ C57BL/6 mice (n = 5) treated with PBS (control) or 6C5. The data are presented as the means ± SEMs, and two or three independent experiments were performed. Statistical analysis of the tumor growth curves was performed via two-way ANOVA. For (c), an unpaired two-tailed t-test was applied. ns not significant, **P < 0.01, ***P < 0.001, and ****P < 0.0001

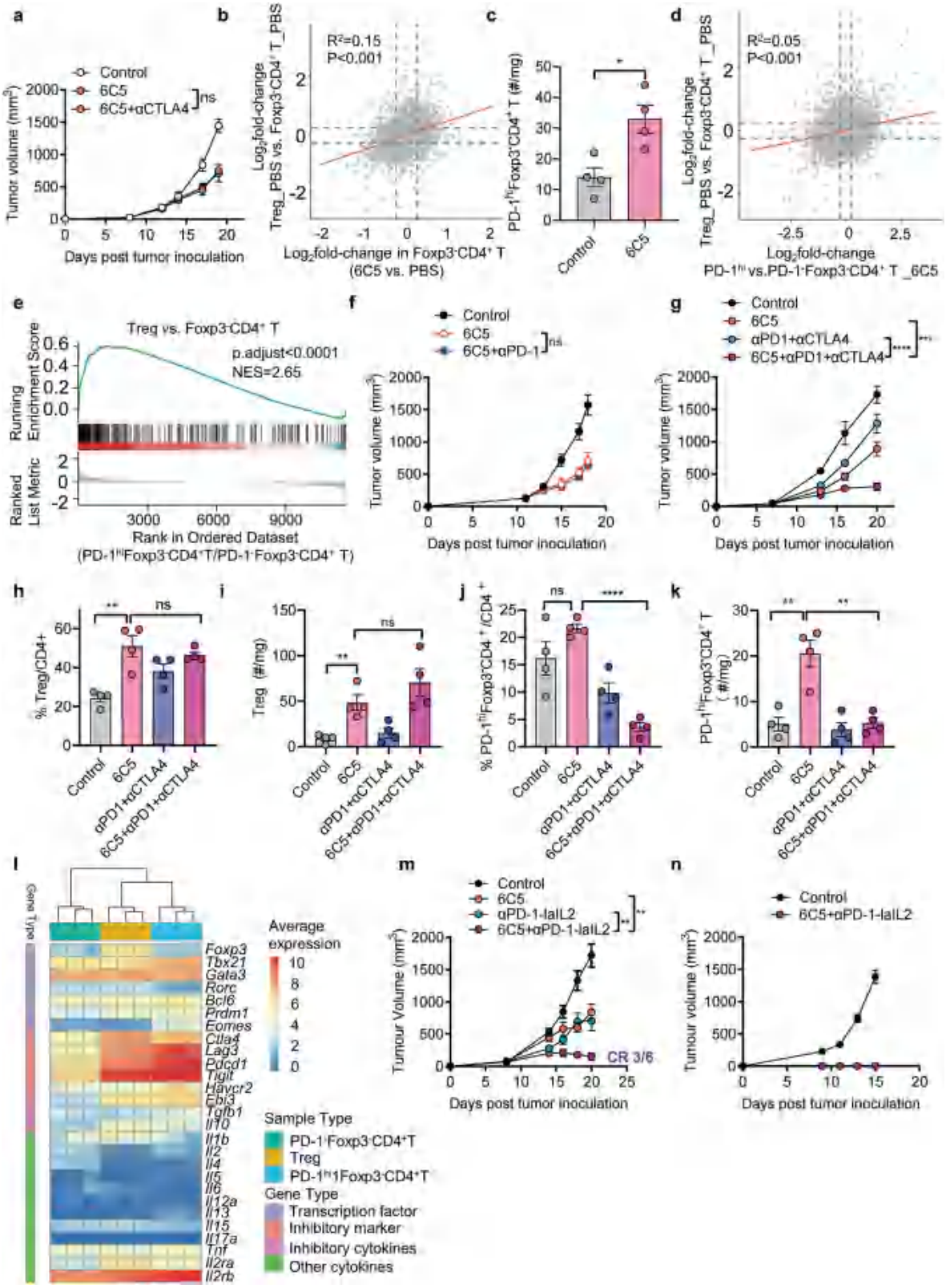

1^{hi} and PD-1^{-}Foxp3^{-}CD4^{+} T cells from the 6C5-treated group were positively correlated with global differences in gene expression between intratumoral Tregs and Foxp3^{-}CD4^{+} T cells from the PBS-treated group (Fig. 6d). Consistently, gene set enrichment analysis (GSEA) of global gene expression differences between PD-1^{hi} and PD-1^{-}Foxp3^{-}CD4^{+} T cells revealed an enrichment of genes upregulated in Treg cells compared with Foxp3^{-}CD4^{+} T cells within the PD-1^{hi} population (Fig. 6e), further suggesting that PD-1 expression is associated with Foxp3^{-}CD4^{+} T cells enriched with a Treg cell–like transcriptional profile.

Fig. 6 The 6C5 antibody overcomes melanoma resistance to immune checkpoint inhibitors. a Tumor growth curves of B16-hAXL-bearing C57BL/6 mice (n = 5) treated with PBS (control), 6C5, or 6C5 + αCTLA4. b Scatterplot comparing the global differences in gene expression between intratumoral Treg cells and Foxp3$^-$CD4$^+$ T cells from the PBS-treated group and the transcriptional differences between intratumoral Foxp3$^-$CD4$^+$ T cells treated with PBS and those treated with 6C5. c The number of intratumoral PD-1^{hi}Foxp3$^-$CD4$^+$ T cells was analyzed in B16-hAXL-bearing C57BL/6 mice that were treated with PBS or 6C5. d Scatterplot comparing the global changes in gene expression between intratumoral Tregs and Foxp3$^-$CD4$^+$ T cells from the PBS-treated group and the transcriptional differences between intratumoral PD-1^{hi}- and PD-1$^-$Foxp3$^-$CD4$^+$ T cells from 6C5-treated mice. e GSEA demonstrating an enrichment of genes upregulated in Treg cells versus Foxp3$^-$CD4$^+$ T cells from the PBS-treated group among PD-1^{hi}Foxp3$^-$CD4$^+$ T cells compared with PD-1$^-$Foxp3$^-$CD4$^+$ T cells isolated from the tumors of 6C5-treated mice. f Tumor growth curves of B16-hAXL-bearing C57BL/6 mice (n = 6) treated with PBS (control), 6C5, or 6C5+anti-PD-1. g Tumor growth curves of B16-hAXL-bearing C57BL/6 mice treated with PBS (control, n = 5), 6C5 (n = 5), αPD-1 + αCTLA4 (n = 7), or 6C5 + αPD-1 + αCTLA4 (n = 8). h–k The frequency and number of intratumoral Tregs and PD-1^{hi}Foxp3$^-$CD4$^+$ T cells were analyzed in B16-hAXL-bearing C57BL/6 mice treated with PBS (control), 6C5, αPD-1 + αCTLA4, or 6C5 + αPD-1 + αCTLA4. l Heatmap depicting the relative expression levels of the indicated gene sets among three intratumoral CD4$^+$ T-cell subsets. m Tumor growth curves of B16-hAXL-bearing C57BL/6 mice treated with PBS (control, n = 5), 6C5 (n = 5), αPD-1-IaIL2 (n = 7), or 6C5 + αPD-1-IaIL2 (n = 6). n Tumor growth curves of C57BL/6 mice with complete tumor regression after treatment with 6C5 combined with αPD-1-IaIL2, followed by subcutaneous rechallenge with B16-hAXL tumor cells. The data are presented as the means ± SEMs, and two or three independent experiments were performed. Statistical analysis of tumor growth was performed via two-way ANOVA. For (c, h–k), unpaired two-tailed t-tests were applied. ns (not significant), *P < 0.05, **P < 0.01, ***P < 0.001, and ****P < 0.0001

The combination of 6C5 with anti-PD-1 treatment did not result in a significantly enhanced therapeutic effect (Fig. 6f). We subsequently employed a combination therapy of 6C5 with dual immune checkpoint therapy (anti-PD-1 plus anti-CTLA4) in B16-hAXL melanoma (Fig. 6g). Notably, while dual ICIs only slightly inhibited tumor growth, the inclusion of 6C5 substantially improved therapeutic efficacy. Importantly, while individual treatment with 6C5 increased the intratumoral populations of both Tregs and PD-1^{hi}Foxp3$^-$CD4$^+$ T cells (Fig. 6h–k), combination with dual ICIs selectively reduced the proportion and number of PD-1^{hi}Foxp3$^-$CD4$^+$ T cells without significantly reducing the number of Tregs (Fig. 6h–k and Supplementary Fig. 5e). These findings highlighted that AXL Ab treatment synergized with dual ICIs and modulated distinct immunosuppressive CD4$^+$ T cells for tumor control.

We further investigated the suppressive mechanisms of PD-1^{hi}Foxp3$^-$CD4$^+$ T cells. Intratumoral CD4$^+$ T cells were sorted for bulk RNA-seq and TCR sequencing. Transcriptomic profiling revealed that PD-1^{hi}Foxp3$^-$CD4$^+$ T cells exhibit a distinct phenotype characterized by elevated expression of multiple immune checkpoint molecules, including CTLA4 (Ctla4), LAG3 (Lag3), PD-1 (Pdcd1), TIGIT (Tigit), and TIM-3 (Havcr2), as well as increased expression of immunosuppressive cytokines such as TGF-β (Tgfb1) and IL10 (Il10) (Fig. 6l). These results indicate that the PD-1^{hi}Foxp3$^-$CD4$^+$ T subset exhibits a potent immunosuppressive phenotype. TCR sequencing further revealed that the majority of clonotypes within PD-1^{hi}Foxp3$^-$CD4$^+$ T cells were unique to this subset, with minimal overlap with Tregs and even less overlap with PD-1$^-$Foxp3$^-$CD4$^+$ T cells (Supplementary Fig. 5f). The top 10 clonotypes accounted for approximately 40% of the PD-1^{hi}Foxp3$^-$CD4$^+$ T-cell repertoire (Supplementary Fig. 5g), but these dominant clonotypes were present at much lower frequencies or were undetectable in the Treg or PD-1$^-$Foxp3$^-$CD4$^+$ T-cell subset (Supplementary Fig. 5h). Impressively, the top 10 clonotypes in PD-1$^-$Foxp3$^-$CD4$^+$ T cells constituted approximately 80% of that subset (Supplementary Fig. 5g) and were scarcely detected in the other two subsets (Supplementary Fig. 5i). Together, these findings indicate that PD-1^{hi}Foxp3$^-$CD4$^+$ T cells represent a clonally expanded and phenotypically distinct population, with only limited lineage overlap with tumor-infiltrating Tregs, and are largely unrelated to conventional PD-1$^-$Foxp3$^-$CD4$^+$ T cells.

The proinflammatory cytokines produced by CD4$^+$ T helper cells play crucial roles in the antitumor immune response.[39] Among these cytokines, interleukin-2 (IL-2) is a pivotal cytokine that significantly influences the proliferation and activation of CD8$^+$ T cells.[40] To overcome the possible IL-2 insufficiency caused by the increase in intratumoral Tregs and PD-1^{hi}Foxp3$^-$CD4$^+$ T cells induced by 6C5 treatment, we administered anti-PD-1-IaIL2 to specifically deliver a low-affinity IL-2 variant into the TME.[41] Notably, combination therapy with 6C5 and anti-PD-1-IaIL2 resulted in significantly enhanced tumor control and complete tumor regression in approximately 50% of the treated mice (Fig. 6m).

CD4$^+$ T-cell depletion has been previously shown to increase the efficacy of cancer immunotherapy but to compromise the development of antitumor immune memory.[42] Similarly, in our study, it markedly amplified the antitumor activity of the membrane-proximal AXL-targeting antibody 6C5 (Fig. 3j) but failed to reject tumor rechallenge (Supplementary Fig. 5j), indicating a loss of durable immune protection. Impressively, all the mice that achieved complete tumor regression following treatment with 6C5 and anti-PD-1-IaIL2 remained fully protected upon rechallenge (Fig. 6n). These findings suggest that combining AXL-targeted therapy with anti-PD-1-IaIL2 therapy effectively counteracts immunosuppressive CD4$^+$ T cells without depleting immune-supportive subsets, which would otherwise compromise immune memory, thereby achieving both robust tumor control and long-lasting immune protection.

DISCUSSION

ICI's clinical benefit remains largely confined to immune-inflamed tumors, whereas immune-cold tumors are intrinsically resistant due to insufficient T-cell priming and infiltration. AXL signaling has been implicated as a key driver of tumor progression, immune evasion, and resistance to immunotherapy, making it an attractive but challenging therapeutic target. Despite extensive efforts to inhibit AXL signaling through receptor tyrosine kinase inhibitors, antibodies, aptamers, or decoy receptors, clinical efficacy has been limited. This failure is often attributed to incomplete blockade and insufficient immune engagement. Here, we developed an anti-AXL antibody (6C5), which specifically binds to the membrane-proximal epitope of AXL and has improved immune-dependent therapeutic efficacy. The 6C5 antibody engages Fc-mediated effector functions to activate macrophages and DCs, which coordinate to recruit and activate antitumor CD8$^+$ T cells. This distinct immunologic modulation overcomes the resistance of immune-cold tumors to ICIs.

Accumulating evidence suggests that the specific location of an antibody-binding epitope is a critical determinant in inducing antibody-dependent cellular antitumor effects. Specifically, antibodies targeting membrane-proximal domains tend to be more effective at triggering NK cell-mediated cytotoxicity or macrophage-mediated phagocytosis. This phenomenon has been observed across various targets, including hematologic

malignancy marker[43] CD20 and solid tumor antigens such as HER2, Glypican-3.[44,45] Notably, antibodies directed against membrane-proximal regions of different tumor antigens do not uniformly elicit the same antibody-dependent immune effector mechanisms. For example, trastuzumab targeting HER2 can elicit both ADCP and ADCC,[46] whereas membrane-proximal targeting of MSLN preferentially enhances ADCC without significantly augmenting ADCP.[47] In our study, the therapeutic efficacy of the membrane-proximal AXL antibody 6C5 was predominantly dependent on macrophage-mediated ADCP rather than NK cell-mediated ADCC. FcγRIIa is considered the principal Fc receptor driving ADCP,[48] whereas FcγRIIIa predominantly mediates ADCC.[49] Consequently, the distinct patterns of ADCC versus ADCP activation elicited by antibodies likely arise from variations in the recruitment and activation of specific Fcγ receptor subtypes, driven by factors such as antigen structure, epitope geometry, and surface density.

This prophagocytic effect of 6C5 is correlated with improved therapeutic outcomes in vivo, facilitating the uptake of tumor antigens by macrophages and subsequently stimulating the production of IFN-I via the MyD88 pathway. In the melanoma TME, the number of TAMs is significantly greater than that of DCs. Additionally, TAMs demonstrate greater uptake of tumor antigens than DCs do, which may explain why TAMs are the primary producers of IFN-β following 6C5 treatment. IFN-I can induce chemokines to recruit immune cells or activate DCs for T-cell activation. Thus, it is a critical molecule that bridges innate and adaptive immunity. Although tissue-resident macrophages and TAMs can also effectively cross-present antigens and activate $CD8^+$ T cells under certain biological conditions,[50,51] $CD103^+$ DCs are generally regarded as the dominant APCs for cross-presentation. 6C5 lost its antitumor effect in DC-depleted or DC-specific IFNAR-KO mice, indicating that DCs are the key APCs that respond to IFN-I. While anti-AXL antibody treatment expanded the number of tumor-infiltrating $CD8^+$ T lymphocytes within the tumor, contributing to tumor inhibition, $CD4^+$ T cells were also activated but exhibited an immune-inhibitory role. Furthermore, we observed that a subset of PD-1-expressing $Foxp3^-CD4^+$ T cells, in addition to Tregs, inhibited T-cell functions and may play a critical inhibitory role. However, the combination of 6C5 with anti-PD-1 did not yield any additional therapeutic benefits, suggesting that anti-PD-1 therapy alone is inadequate to suppress this population of cells. Previous reports indicate that $Nrp\text{-}1^+CD4^+$ Tconv cells are dysfunctional and exhibit impaired proliferation and the production of fewer proinflammatory cytokines than $Nrp\text{-}1^-CD4^+$ Tconv cells do. Moreover, this population displays elevated levels of PD-1 and CTLA-4 expression.[52] We hypothesize that $PD\text{-}1^{hi}Foxp3^-CD4^+$ T cells may share certain characteristics with $Nrp\text{-}1^+CD4^+$ Tconv cells. Therefore, we combined 6C5 with anti-PD-1 and anti-CTLA4 treatment, which significantly enhanced treatment effectiveness. However, the potential relationship between $Nrp\text{-}1^+CD4^+$ Tconv cells and $PD\text{-}1^{hi}Foxp3^-CD4^+$ T cells warrants further investigation. Moreover, we propose that intratumoral Tregs and $PD\text{-}1^{hi}Foxp3^-CD4^+$ T cells may inhibit antitumor $CD8^+$ T lymphocytes through the consumption of IL-2. The recently developed anti-PD-1-IalL2 agent is a new generation of ICIs that selectively delivers IL-2 into the TME to expand preexisting T cells. Here, we demonstrate that the combination of 6C5 and anti-PD-1-IalL2 not only markedly enhances antitumor efficacy but also promotes the establishment of durable immunological memory. Future studies should also further define the origin, differentiation state, and APC requirements of the $PD\text{-}1^{hi}Foxp3^-CD4^+$ T-cell population, as well as determine how these cells can be selectively neutralized without broadly compromising immune activation. In our experiments, although global depletion of $CD4^+$ T cells markedly enhanced therapeutic efficacy and even resulted in tumor regression in a subset of cases, it failed to elicit durable immunological memory. These findings indicate that the $CD4^+$ T-cell compartment contains not only immunosuppressive subsets but also helper populations that are essential for memory formation. Consequently, identifying specific markers that uniquely define $PD\text{-}1^{hi}Foxp3^-CD4^+$ T cells and developing depleting antibodies that selectively target this population will be critical for maximizing therapeutic benefit while preserving long-term antitumor immunity.

Given the dependency of anti-AXL treatment on APCs, further exploration of combination strategies with myeloid-stimulating agents such as agonistic anti-CD40 antibodies that enhance macrophage polarization toward an antitumor phenotype and amplify phagocytosis and antigen presentation is needed.[53] Because 6C5 can induce macrophage-mediated uptake of tumor antigens, an additional strategy would be to conjugate 6C5 with Toll-like receptor or STING agonists to generate an immunostimulatory ADC, which could further enhance intratumoral macrophage activation and more effectively remodel the TME. At the same time, it is important to consider whether antibodies targeting distinct AXL epitopes differ in their internalization efficiency by tumor cells, as this parameter is critical for the efficacy of toxin-conjugated ADC. Notably, AXL expression is not tumor-restricted, and prior clinical studies have reported significant toxicities associated with AXL-directed ADC carrying cytotoxic payloads. Engineering AXL antibodies with selective binding to AXL in a TME–restricted manner may thus provide a viable strategy to mitigate the dose-limiting toxicities associated with conventional AXL-directed ADC.[54]

In summary, antibodies targeting the membrane-proximal domain of AXL elicit potent antitumor activity primarily through macrophage-mediated ADCP, which initiates a cascade of IFN-I–driven DC activation and cytotoxic T-cell priming. These findings highlight their potential to mediate innate immunity and activate the adaptive immune response to convert "immune-cold" tumors to "immune-hot" tumors. The mechanistic insights revealed here create new opportunities to leverage these immune modulations to overcome resistance to both conventional and next-generation ICIs therapy.

MATERIALS AND METHODS

Mice

BALB/c and C57BL/6 mice were purchased from Vital River Laboratories (Beijing, China). The CD11c-DTR, Zbtb46-cre, Lyz2-cre, $Ifnar1^{f/f}$, $Ifnar1^{-/-}$, $Tmem173^{-/-}$, $Myd88^{-/-}$, $Batf3^{-/-}$, NSG-SGM3, and $Rag1^{-/-}$ mice were bred and maintained at the animal facility at Tsinghua University. The mAxl knockout C57BL/6 mice and hAXL-transgenic C57BL/6 mice were developed by Dr. Liguo Zhang's laboratory. Mice aged 6–8 weeks were used for all the experiments. All the mice were maintained under specific pathogen-free conditions in the animal facilities of the Institute of Biophysics (IBP), Chinese Academy of Sciences (CAS), and Tsinghua University. Animal care and experiments were carried out under institutional protocols and guidelines. All studies were approved by the Animal Care and Use Committee of the IBP (SYXK2021070), CAS, and Tsinghua University (21-FYX1.G24-1).

Cell lines

The B16-hAXL, MC38-hAXL, and CT26-hAXL cell lines were derived through transfection with a lentivirus expressing hAXL. The MC38, B16F10, CFPAC-1, Calu-1, SN12C, B16-hAXL, and MC38-hAXL cell lines were maintained in Dr. Liguo Zhang's laboratory. The MC38, B16F10, B16-hAXL, MC38-hAXL, and CFPAC-1 cell lines were cultured in Dulbecco's modified Eagle's medium (DMEM) supplemented with 10% heat-inactivated fetal bovine serum (FBS), 2 mM L-glutamine, 50 U/ml penicillin, and 50 μg/ml streptomycin. CT26-hAXL, SN12C, and Calu-1 cells were cultured in RPMI-1640 medium supplemented with 10% FBS, 2 mM L-glutamine, 50 U/ml penicillin, and 50 μg/ml streptomycin. All the cell lines were cultured at 37 °C in 5% CO_2.

Antibodies and reagents

All antibodies targeting hAXL were developed and screened in Dr. Liguo Zhang's laboratory. Briefly, The mAXL knockout BALB/c mice were immunized monthly with L929 cells expressing hAXL or AXL truncations supplemented with CpG1826 (Thermo Fisher Scientific). Serum from the immunized mice was analyzed for reactivity toward hAXL-expressing HEK293T cells via flow cytometry. Hybridoma formation was conducted following previously established protocols. Three days after the final boost immunization (without adjuvant), splenocytes from the immunized mice were isolated and fused with SP2/0 myeloma cells via 50% polyethylene glycol (PEG) 4000 (Sigma-Aldrich). The cells were subsequently plated in 96-well plates containing hypoxanthine/aminopterin/thymidine (HAT) medium (Sigma-Aldrich) with feeder cells (peritoneal macrophages) that had been seeded 24 h earlier. The hybridoma culture supernatants were screened via flow cytometry with hAXL-expressing HEK293T cells on an Attune NxT flow cytometer (Thermo Fisher Scientific). Positive hybridomas were subcloned, and this process was repeated for four additional rounds until a 100% positive rate was achieved. Finally, the antibodies were produced in the ascites of NSG mice and purified via a protein A agarose column.

Anti-NK1.1 antibody (clone PK136), anti-CD8 antibody (TIB210), anti-CD4 antibody (GK1.5), anti-CSF1R antibody (AFS98), anti-IFNAR1 antibody (MAR1-5A3), anti-PD-1 antibody (J43), and anti-CTLA4 antibody (9D9) were purchased from Bio X Cell (USA). AF700 anti-CD45 antibody (30-F11), APC-Cy7 anti-CD45 antibody (30-F11), PE anti-CD3 antibody (17A2), FITC anti-CD19 antibody (1D3/CD19), APC-Cy7 anti-CD4 antibody (GK1.5), PE-Cy7 anti-CD8a antibody (53-6.7), BV421 anti-CD11b antibody (M1/70), PerCP-Cy5.5 anti-NK1.1 antibody (PK136), FITC anti-PD-1 antibody (29F.1A12), PE-Cy7 anti-CD11c antibody (N418), AF700 anti-IA/IE antibody (M5/114.15.2), BV421 anti-CD11b antibody (M1/70), and PE anti-F4/80 antibody (BM8) were purchased from Biolegend. APC anti-4-1BB antibody (17B5), BV650 anti-F4/80 antibody (BM8), APC anti-Foxp3 antibody (FJK-16 s), PerCP-Cy5.5 anti-Ly6C antibody (HK1.4), and purified mouse IgG2a (MG2a-53) were purchased from Invitrogen.

The following monoclonal antibodies were obtained from ABclonal Technology: phospho-Axl-Y702 rabbit mAb (cat#. AP1427), rabbit Axl rabbit mAb (cat#. A22378), phospho-Akt-S473 rabbit mAb (cat#. AP1208), anti-pan-Akt rabbit mAb (cat#. A18675), and the following antibodies were obtained from ZSGB-BIO: mouse anti-β-actin mAb (cat#. TA-09), horseradish enzyme-labeled goat anti-rabbit IgG (H + L) polyclonal (cat#. ZB-2301), horseradish enzyme-labeled goat anti-mouse IgG (H + L) polyclonal (cat#. ZB-2305). A mouse IFN-β ELISA kit (439407) was purchased from Biolegend.

Tumor inoculation and treatments

B16-hAXL (1×10^5 to 1×10^6), MC38-hAXL (2×10^5), CT26-hAXL (3×10^5), and B16F10 (2×10^5) cells were subcutaneously implanted into the right flanks of 6- to 8-week-old mice. The tumor volume was measured two to three times per week and calculated via the formula length × width^2/2. Once the tumors were established, the mice received intraperitoneal injections of either PBS or 200 μg of anti-AXL every 3 days for a total of 3 to 4 doses unless otherwise specified. Additionally, for combination therapy, 200 μg of anti-PD-1 (J43) or anti-CTLA4 (9D9) was administered intraperitoneally every 3 days. Alternatively, 20 μg of anti-PD-1-IL-2 was injected intraperitoneally every 3 days. To block IFN-I signaling, 100 μg of anti-IFNAR1 (clone MAR1-5A3) was administered intratumorally once every 3 days. For the depletion of $CD8^+$ T cells, $CD4^+$ T cells, macrophages, NK cells, 200 μg of anti-CD8 antibody (TIB210), anti-CD4 antibody (GK1.5), anti-CSF1R antibody (AFS98), or anti-NK1.1 antibody (PK136) were injected intraperitoneally, starting with 6C5 treatment every 3 days for a total of three doses. $CD11c^+$ cells were depleted in mice that received CD11c-DTR cells via the intraperitoneal injection of diphtheria toxin (DT; 200 ng per mouse). To establish humanized mouse models, NSG-SGM3 mice received an intravenous injection of 1×10^7 human PBMCs (MileCell Biotechnology) on day 8 following tumor implantation.

Flow cytometry

Tumor tissues were harvested, minced into small fragments, digested in RPMI-1640 with 1 mg/mL collagenase type IV (Sigma–Aldrich) and 0.5 mg/mL DNase I (Roche) at 37 °C for 30 min, and then passed through a 70 μm cell strainer to make single-cell suspensions. The cells were subsequently blocked with anti-mouse CD16/32 antibody (clone 2.4G2) for 20 min and then stained with specific antibodies for 30 min at 4 °C. For intracellular Foxp3 staining, the cells were fixed and permeabilized via the Foxp3/Transcription Factor Staining Buffer Set (eBioscience, 00-5523-00), followed by staining with anti-mouse Foxp3. Dead cells were excluded via a LIVE/DEAD Fixable Aqua Dead Cell Stain Kit (Thermo Fisher Scientific, L34957). Flow cytometry was performed via a BD LSRFortessa™ flow cytometer, and the data were analyzed with FlowJo software (Tree Star).

Macrophage differentiation and phagocytosis assays

Mouse macrophages were differentiated from the bone marrow cells of C57BL/6 mice. Unfractionated bone marrow cells were cultured in DMEM supplemented with 10% FBS, 2 mM L-glutamine, 50 U/ml penicillin, 50 μg/ml streptomycin, and 50 ng/ml murine M-CSF (Novoprotein, CB34). The medium was changed on days 3 and 5, and the cells were collected on day 7.

For the in vitro phagocytosis experiment, B16-hAXL tumor cells were labeled with 5 μm CFSE. Subsequently, in a 24-well plate, 2×10^5 labeled B16-hAXL cells were added per well, followed by the addition of 1×10^5 bone marrow-derived macrophages at a ratio of 2:1. AXL antibody was introduced to achieve a final concentration of 10 μg/ml, and the mixture was incubated in a 37 °C incubator with 5% CO_2. After 2 h of incubation, the macrophages were labeled with a PE-conjugated anti-F4/80 antibody and quantified via flow cytometry.

Assessment of AXL antibody-binding capacity to tumor cells

The tumor cells were washed once with FACS buffer and filtered through a 70-μm cell strainer. The single-cell suspensions were blocked with an anti-mouse CD16/32 antibody (clone 2.4G2; BioLegend) for 20 min at 4 °C. Then, the anti-AXL antibodies were serially diluted and incubated with the tumor cells at 4 °C for 30 min. After two washes with FACS buffer, the cells were stained with a PE-conjugated anti-mouse IgG secondary antibody (BioLegend, 407108) for 30 min at 4 °C in the dark, and flow cytometry was performed.

Western blotting

Calu-1 cells were serum-starved overnight and then pretreated for 1.5 h with 100 μg/mL of 6C5, αAXL-1#, or 6S2; purified mouse IgG2a (Clone MG2a–53); or 5 μM R428. The cells were subsequently stimulated with 200 ng/mL Gas6 for 30 min. After being washed with cold PBS, the cells were lysed in CelLytic™ M Cell Lysis Buffer (Sigma-Aldrich, C2978) supplemented with cOmplete™ Mini Protease Inhibitor Cocktail (Roche, 04693124001) and Phosphatase Inhibitor Cocktail (Beyotime, P1082). The lysates were separated by 10% SDS-PAGE and transferred to Immobilon-FL PVDF membranes (EMD Millipore). The membranes were incubated overnight at 4 °C with primary antibodies targeting total Axl, phospho-Axl (Y702), total Akt, phospho-Akt (S473), or β-actin. Following washes, the membranes were incubated with appropriate HRP-conjugated secondary antibodies (anti-rabbit or anti-mouse). The protein bands were visualized via a Mini Chemiluminescent Imaging and Analysis System.

Single-cell RNA-sequencing and analysis

C57BL/6 mice (n = 4 per group) were inoculated with B16-hAXL cells and treated with either PBS or 200 μg of 6C5 by intraperitoneal injection on days 11 and 14. Tumor tissues were collected and digested on day 15. $CD45^+$ cells were sorted via flow cytometry. Single-cell RNA-seq libraries were prepared via the Chromium Single-cell Reagent Kit v3 (10x Genomics) in accordance with the manufacturer's instructions. The cells were captured in droplets to achieve a specific cell recovery rate. Following the reverse transcription step, the emulsions were broken, and the barcoded cDNA was purified with Dynabeads, followed by PCR amplification. The amplified cDNA was then used to construct the gene expression library. For this construction, 50 ng of amplified cDNA was fragmented and end-repaired, double-sized with SPRIselect beads, and sequenced on a NovaSeq platform (Illumina) to generate 150 bp paired-end reads, as per the manufacturer's instructions. Raw data from FASTQ files were generated from the raw BCL files via Illumina's bcl2fastq converter. The raw data were initially processed through primary quality control. The monitored quality assessment parameters included the following: (a) contained more than 3 N bases; (b) the proportion of bases with a quality value less than 5 exceeded 20%; and (c) the presence of adapter sequences. All downstream analyses were conducted on high-quality, clean data. The Seurat R package v5.0.1 was employed for data normalization, dimensionality reduction, unsupervised clustering, and differential expression analysis.

Bulk RNA-seq and TCR sequencing

Smart-seq2 was performed as previously described with minor modifications.[55] For each experiment, a maximum of 20,000 cells were deposited in tubes containing 50 μL of lysis buffer, centrifuged, and immediately frozen at −80 °C. The RNA was purified via RNA clean beads (Vazyme, #N412-01). Reverse transcription was performed via SuperScript II Reverse Transcriptase (Invitrogen, #18064-014), followed by PCR amplification via KAPA HiFi HotStart Ready Mix (Kapa Biosystems, #KK2602). cDNA amplification was followed by two rounds of SPRI purification, and the cDNA concentration was measured with a Qubit fluorometer (Life Technologies). The library was prepared from 1 ng of cDNA via the TruePrepTM DNA Library Prep Kit V2 for Illumina (Vazyme, #TD502), followed by SPRI size selection. TCR sequencing was performed via the Renke TCR repertoire analysis system (Renke Shenzhen Biotechnology Co., Ltd.). To specifically amplify murine TCR sequences, primers targeting the constant region of the TCR β chain were designed and used for nested PCR amplification to construct libraries for next-generation sequencing. Paired-end 150 bp sequencing was performed on an MGI platform.

Statistical analysis

All data analyses were conducted via GraphPad Prism software. The data are presented as the means ± SEMs. Statistical significance is indicated as follows: *P < 0.05, **P < 0.01, ***P < 0.001, ****P < 0.0001, ns not significant.

DATA AVAILABILITY

All data supporting the findings of this study are available within the article and its Supplementary Information files. The bulk RNA-sequencing data (including TCR sequencing data) and single-cell RNA-sequencing datasets generated during this study have been deposited in NCBI's Gene Expression Omnibus (GEO) and are accessible through GEO Series accession numbers GSE314707 (bulk RNA-seq) and GSE319111 (scRNA-seq). Uncropped original Western blot images are provided as Supplementary Data S1.

ACKNOWLEDGEMENTS

The authors are grateful to Hua Peng (Guangzhou National Laboratory) for providing IFNAR-flox mice, Li Wu (Tsinghua University) for providing Zbtb46-Cre mice, and Xiaoyu Hu (Tsinghua University) for providing Lyz2-Cre mice. The authors acknowledge the staff at the animal facilities of the IBP, CAS, and Tsinghua University. Schematic diagrams of mouse treatment were generated via BioRender. This work was supported by grants from the National Natural Science Foundation of China (82371853 to X.Z., 82250710684 to Y.F.), funding from the National Science and Technology Major Project of the Ministry of Science and Technology of China (2023YFC2508505 to Y.L.), and funding from the Chinese Academy of Sciences (CAS) grants (Strategic Priority Research Program XDB1310000 to L.Z.).

AUTHOR CONTRIBUTIONS

Z.Y., X.Z., and Y.L. conceived and designed the research. X.Z. and X.N. performed the antibody screening and validation. Z.Y., S.C., J.Z., J.W., and H.H. conducted the animal tumor studies. Ex vivo and in vivo mechanistic investigations were carried out by Z.Y., S.C., and J.Z. Z.W. and X.S. contributed to the bioinformatics analyses. X.Z. and J.W. constructed and validated the hAXL-transgenic mice and $Axl^{-/-}$ mice. J.Z., S.Y., X.K., Z.W., P.D., M.T., L.Z., Z.R., and X.L. provided essential biological materials for this study. Y.L., X.Z., L.Z., and Y.F. supervised the project and directed the research. Z.Y. authored the manuscript. Y.L., X.Z., L.Z., and Y.F. edited and revised the manuscript. All the authors have read and approved the article.

ADDITIONAL INFORMATION

Supplementary information The online version contains supplementary material available at https://doi.org/10.1038/s41392-026-02664-x.

Competing interests: X.Z., X.N., Z.Y., and L.Z. are listed as inventors on a patent application (Patent Application Number: CN2024115456701) for anti-AXL antibodies. The other authors declare that they have no competing interests.

Publisher's note Springer Nature remains neutral with regard to jurisdictional claims in published maps and institutional affiliations.

REFERENCES

1. Yin, N. et al. Development of pharmacological immunoregulatory anti-cancer therapeutics: current mechanistic studies and clinical opportunities. Signal Transduct. Target. Ther. 9, 126 (2024).
2. Wu, B. et al. Cold and hot tumors: from molecular mechanisms to targeted therapy. Signal Transduct. Target. Ther. 9, 274 (2024).
3. Liu, Y. T. et al. Turning cold tumors into hot tumors to ignite immunotherapy. Mol. Cancer 24, 254 (2025).
4. Albert, G. K., Cao, P. & Davila, E. Leveraging innate immune signals in CD8+ T cells to boost antitumor immunity. Front. Immunol. 16, 1617773 (2025).
5. Gajewski, T. F., Schreiber, H. & Fu, Y. X. Innate and adaptive immune cells in the tumor microenvironment. Nat. Immunol. 14, 1014–1022 (2013).
6. Liu, Y., Xu, L., Dou, Y. & He, Y. AXL:shapers of tumor progression and immunosuppressive microenvironments. Mol. Cancer 24, 11 (2025).
7. Rothlin, C. V. et al. TAM receptors are pleiotropic inhibitors of the innate immune response. Cell 131, 1124–1136 (2007).
8. Yadav, M. et al. AXL signaling in cancer: from molecular insights to targeted therapies. Signal Transduct. Target. Ther. 10, 37 (2025).
9. Skinner, H. D. et al. Integrative analysis identifies a novel AXL-PI3 kinase-PD-L1 signaling axis associated with radiation resistance in head and neck cancer. Clin. Cancer Res. 23, 2713–2722 (2017).
10. Terry, S. et al. Association of AXL and PD-L1 expression with clinical outcomes in patients with advanced renal cell carcinoma treated with PD-1 blockade. Clin. Cancer Res. 27, 6749–6760 (2021).
11. Wu, X. et al. AXL-GAS6 expression can predict for adverse prognosis in non-small cell lung cancer with brain metastases. J. Cancer Res. Clin. Oncol. 143, 1947–1957 (2017).
12. Yu, H. et al. Axl receptor tyrosine kinase is a potential therapeutic target in renal cell carcinoma. Br. J. Cancer 113, 616–625 (2015).
13. Bae, C. A. et al. Inhibiting the GAS6/AXL axis suppresses tumor progression by blocking the interaction between cancer-associated fibroblasts and cancer cells in gastric carcinoma. Gastric Cancer 23, 824–836 (2020).
14. Antony, J. et al. The tumour suppressor OPCML promotes AXL inactivation by the phosphatase PTPRG in ovarian cancer. EMBO Rep. 19, e45670 (2018).
15. Jin, G. et al. Expression of Axl and its prognostic significance in human breast cancer. Oncol. Lett. 13, 621–628 (2017).

16. Boshuizen, J. et al. Cooperative targeting of melanoma heterogeneity with an AXL antibody-drug conjugate and BRAF/MEK inhibitors. Nat. Med. 24, 203–212 (2018).
17. DeRyckere, D., Huelse, J. M., Earp, H. S. & Graham, D. K. TAM family kinases as therapeutic targets at the interface of cancer and immunity. Nat. Rev. Clin. Oncol. 20, 755–779 (2023).
18. Liu, Z. et al. Recent discovery and development of AXL inhibitors as antitumor agents. Eur. J. Med. Chem. 272, 116475 (2024).
19. Vandewalle, N. et al. AXL-specific single domain antibodies show diagnostic potential and anti-tumor activity in Acute Myeloid Leukemia. Theranostics 14, 2656–2674 (2024).
20. Chang, H. et al. Anti-Axl monoclonal antibodies attenuate the migration of MDA-MB-231 breast cancer cells. Oncol. Lett. 22, 749 (2021).
21. Chen, T. J. et al. AXL targeting by a specific small molecule or monoclonal antibody inhibits renal cell carcinoma progression in an orthotopic mice model. Physiol. Rep. 9, e15140 (2021).
22. Bonifacio, L. et al. Target-mediated drug disposition pharmacokinetic/pharmacodynamic model-informed dose selection for the first-in-human study of AVB-S6-500. Clin. Transl. Sci. 13, 204–211 (2020).
23. Ye, X. et al. An anti-Axl monoclonal antibody attenuates xenograft tumor growth and enhances the effect of multiple anticancer therapies. Oncogene 29, 5254–5264 (2010).
24. Leconet, W. et al. Therapeutic activity of anti-AXL antibody against triple-negative breast cancer patient-derived xenografts and metastasis. Clin. Cancer Res. 23, 2806–2816 (2017).
25. Galvez-Cancino, F. et al. Fcγ receptors and immunomodulatory antibodies in cancer. Nat. Rev. Cancer 24, 51–71 (2024).
26. Yin, Z. et al. Detection of Gas6/AXL complex and its expression changes in patients with ST-segment elevation myocardial infarction. Front. Med. 12, 1653708 (2025).
27. Myers, K. V., Amend, S. R. & Pienta, K. J. Targeting Tyro3, Axl and MerTK (TAM receptors): implications for macrophages in the tumor microenvironment. Mol. Cancer 18, 94 (2019).
28. Lemke, G. Biology of the TAM receptors. Cold Spring Harb. Perspect. Biol. 5, a009076 (2013).
29. Rankin, E. B. & Giaccia, A. J. The receptor tyrosine kinase AXL in cancer progression. Cancers 8, 103 (2016).
30. Khan, S. M. et al. Impact of CD4 T cells on intratumoral CD8 T-cell exhaustion and responsiveness to PD-1 blockade therapy in mouse brain tumors. J. Immunother. Cancer 10, e005293 (2022).
31. Ferris, S. T. et al. cDC1 prime and are licensed by CD4(+) T cells to induce anti-tumour immunity. Nature 584, 624–629 (2020).
32. Burnette, B. C. et al. The efficacy of radiotherapy relies upon induction of type i interferon-dependent innate and adaptive immunity. Cancer Res. 71, 2488–2496 (2011).
33. Woo, S. R. et al. STING-dependent cytosolic DNA sensing mediates innate immune recognition of immunogenic tumors. Immunity 41, 830–842 (2014).
34. de Queiroz, N. et al. MyD88-dependent BCG immunotherapy reduces tumor and regulates tumor microenvironment in bladder cancer murine model. Sci. Rep. 11, 15648 (2021).
35. Mizutani, T. et al. Conditional IFNAR1 ablation reveals distinct requirements of Type I IFN signaling for NK cell maturation and tumor surveillance. Oncoimmunology 1, 1027–1037 (2012).
36. Li, S. et al. IL-1β expression in bone marrow dendritic cells is induced by TLR2 agonists and regulates HSC function. Blood 140, 1607–1620 (2022).
37. Larson-Casey, J. L. et al. Macrophage Akt1 kinase-mediated mitophagy modulates apoptosis resistance and pulmonary fibrosis. Immunity 44, 582–596 (2016).
38. Zappasodi, R. et al. Non-conventional inhibitory CD4(+)Foxp3(-)PD-1(hi) T cells as a biomarker of immune checkpoint blockade activity. Cancer Cell 33, 1017–1032.e1017 (2018).
39. Kim, H. J. & Cantor, H. CD4 T-cell subsets and tumor immunity: the helpful and the not-so-helpful. Cancer Immunol. Res. 2, 91–98 (2014).
40. Moynihan, K. D. et al. IL2 Targeted to CD8+ T cells promotes robust effector T-cell responses and potent antitumor immunity. Cancer Discov. 14, 1206–1225 (2024).
41. Ren, Z. et al. Selective delivery of low-affinity IL-2 to PD-1+ T cells rejuvenates antitumor immunity with reduced toxicity. J. Clin. Investig. 132, e153604 (2022).
42. Jing, W., Gershan, J. A. & Johnson, B. D. Depletion of CD4 T cells enhances immunotherapy for neuroblastoma after syngeneic HSCT but compromises development of antitumor immune memory. Blood 113, 4449–4457 (2009).
43. Cleary, K. L. S. et al. Antibody distance from the cell membrane regulates antibody effector mechanisms. J. Immunol. 198, 3999–4011 (2017).
44. Nakano, K. et al. Anti-glypican 3 antibodies cause ADCC against human hepatocellular carcinoma cells. Biochem. Biophys. Res. Commun. 378, 279–284 (2009).
45. Weisser, N. E. et al. An anti-HER2 biparatopic antibody that induces unique HER2 clustering and complement-dependent cytotoxicity. Nat. Commun. 14, 1394 (2023).
46. Panaampon, J. et al. Trastuzumab, a monoclonal anti-HER2 antibody modulates cytotoxicity against cholangiocarcinoma via multiple mechanisms. Int. Immunopharmacol. 138, 112612 (2024).
47. Hatterer, E. et al. Targeting a membrane-proximal epitope on mesothelin increases the tumoricidal activity of a bispecific antibody blocking CD47 on mesothelin-positive tumors. MAbs 12, 1739408 (2020).
48. Richards, J. O. et al. Optimization of antibody binding to FcgammaRIIa enhances macrophage phagocytosis of tumor cells. Mol. Cancer Ther. 7, 2517–2527 (2008).
49. Wöhner, M. & Nimmerjahn, F. Cytotoxic IgG: mechanisms, functions, and applications. Immunity 58, 1378–1395 (2025).
50. Bernhard, C. A., Ried, C., Kochanek, S. & Brocker, T. CD169+ macrophages are sufficient for priming of CTLs with specificities left out by cross-priming dendritic cells. Proc. Natl. Acad. Sci. USA 112, 5461–5466 (2015).
51. Muraoka, D. et al. Antigen delivery targeted to tumor-associated macrophages overcomes tumor immune resistance. J. Clin. Investig. 129, 1278–1294 (2019).
52. Abberger, H. et al. Neuropilin-1 is expressed on highly activated CD4(+) effector T cells and dysfunctional CD4(+) conventional T cells from naive mice. J. Immunol. 207, 1288–1297 (2021).
53. Liu, P. S. et al. Author Correction: CD40 signal rewires fatty acid and glutamine metabolism for stimulating macrophage anti-tumorigenic functions. Nat. Immunol. 24, 1591 (2023).
54. Chang, H. W. et al. Preclinical development of mecbotamab vedotin (BA3011), a novel, AXL-specific conditional active biologic antibody-drug conjugate. Antib. Ther. 8, 145–156 (2025).
55. Trombetta, J. J. et al. Preparation of single-cell RNA-seq libraries for next generation sequencing. Curr. Protoc. Mol. Biol. 107, 4.22.21–24.22.17 (2014).